Prediction of Transonic Buffet by Delayed Detached-Eddy Simulation

Fernando Grossi* and Marianna Braza†
Institut de Mécanique des Fluides de Toulouse - UMR 5502, Toulouse, France
Yannick Hoarau‡
Laboratoire des sciences de l'ingénieur, de l'informatique et de l'imagerie - UMR 7357, Strasbourg, France

A Delayed Detached-Eddy Simulation of the transonic buffet over a supercritical airfoil is performed. The turbulence modeling approach is based on a one-equation closure and the results are compared to a URANS simulation using the same baseline model as well as to experimental data. The DDES successfully predicts the self-sustained shock-wave/boundary layer interaction associated with buffet. When separation occurs, the flow exhibits alternate vortex shedding and a spanwise undulation. The method also captures secondary fluctuations in the boundary layer which are not predicted by URANS. Statistical pressure distributions and velocity profiles are in good agreement with the experiments. A map of flow separation emphasizes the differences between the DDES and URANS flow topologies. Instantaneous distributions of RANS and LES regions during buffet show that the DDES enforces RANS mode near the airfoil even when the boundary layer gets very thick.

Nomenclature

a	Local speed of sound
c	Airfoil chord
c_L	Lift coefficient
c_p	Pressure coefficient
d	Wall distance
f	Buffet frequency, Hz
p	Static pressure
$\|S\|$	Euclidean norm of the strain rate tensor
t	Physical time
T	Buffet period
u	Longitudinal component of velocity
U	Freestream velocity magnitude
v	Vertical component of velocity
x	Coordinate parallel to the chord
y	Coordinate in the vertical direction
y^+	Non-dimensional wall distance
z	Coordinate in the spanwise direction
α	Angle of attack
Δ	Grid spacing
ν	Kinematic viscosity
ν_t	Eddy viscosity
$\|\Omega\|$	Euclidean norm of the vorticity tensor

I. Introduction

Aircraft flying at transonic speeds may be submitted to vibrations of aerodynamic origin that appear under specific combinations of Mach number and incidence. The phenomenon results from a flow instability commonly known as transonic buffet and is driven by sufficiently strong shock waves and boundary layer separation. The resulting unsteady shock wave/boundary layer interaction is characterized by self-sustained shock oscillations of large amplitude and can therefore cause intense fluctuations of lift, thus affecting manoeuvrability and limiting the flight envelope of an aircraft. Detailed experiments focused on transonic buffet were first performed by McDevitt et al.[1] and Seegmiller et al.[2] on a circular-arc airfoil. Regarding supercritical profiles, the phenomenon has been

*Ph.D. Student, Institut National Polytechnique de Toulouse; grossi@imft.fr.
†Directrice de Recherche, Centre National de la Recherche Scientifique; braza@imft.fr.
‡Maître de Conférences, Université de Strasbourg; hoarau@unistra.fr.

intensively investigated over the years as in the works by Roos[3], Lee[4], Lee and Tang[5] and more recently by Jacquin et al.[6]. The physics governing transonic buffet is complex and remains to be clarified, though several theories have been proposed. According to one of the most widespread models[7], the phenomenon is explained by means of a wave-propagation feedback mechanism, while a more recent theory[8] links its origin to the onset of a global instability.

While Computational Fluid Dynamics (CFD) techniques may provide considerably accurate results around the cruising design point of an airplane, for example, they become less reliable as one approaches the limits of the flight envelope, where nonlinear effects such as flow separation and shock waves get pronounced. Furthermore, the high Reynolds numbers typical of aerodynamic applications require the use of an appropriate closure for the turbulent stresses and time-resolved computations are frequently necessary. Concerning transonic buffet, the unsteady shock wave/boundary layer interaction represents a major challenge for turbulence models and the low frequencies associated with the shock-wave motion can make the simulations very expensive. Since the pioneering simulations by Levy[9] and Seegmiller et al.[2] for a circular-arc airfoil, Unsteady Reynolds-Averaged Navier-Stokes (URANS) computations using eddy-viscosity turbulence models have been largely used to predict the phenomenon over two-dimensional airfoils, which is a model for the more complex airplane buffet problem[8]. Navier-Stokes simulations of transonic buffet as well as of the shock-vortex interaction at moderate Reynolds numbers were reported by Bouhadji and Braza[10,11].

As a compromise between accuracy and computational cost, the URANS approach has shown the ability to reproduce the basic features of buffeting flows over several types of lifting airfoils[12–15]. However, with the increasing computational resources available, turbulence-resolving methods offering Large Eddy Simulation (LES) capabilities for high-Reynolds number separated flows have emerged, the so-called hybrid RANS-LES methods. An overview of such methods is presented in the review by Fröhlich and von Terzi[16] and examples of recent applications can be found in the collected works after the 3rd and 4th Hybrid RANS-LES Symposia[17,18]. Compared to standard RANS/URANS approaches where the turbulence spectrum is fully modeled, hybrid RANS-LES methods can provide extra level of physical representation through the resolution of part of the turbulent structures. Regarding their application to the transonic buffet problem, Deck[19] performed a Zonal Detached-Eddy Simulation (ZDES) of the unsteady flow over the OAT15A supercritical airfoil in the buffet regime. In that study, the ZDES method was the only model successful in predicting the self-sustained motion of the shock wave near the experimental buffet onset boundary. In the present paper, the same flow is investigated by means of the Delayed Detached-Eddy Simulation (DDES) approach of Spalart et al.[20], which is an improved version of the Detached-Eddy Simulation (DES) method[21] in respect of preventing the switching to LES inside attached boundary layers. It should be recalled, however, that both methods are originally intended to massively separated flows so that the present application should be regarded as an extended use of DDES as the height of the separation region remains small during buffet.

Test case description

The transonic buffet over the OAT15A airfoil was investigated in the experimental work by Jacquin et al.[6] at a freestream Mach number of 0.73 and a chord-based Reynolds number of 3 million. The OAT15A is a supercritical wing section with a thickness-to-chord ratio of 12.3%. The wind tunnel model had a chord of 0.23 m and a blunt trailing edge measuring $0.005\,c$. The airfoil was mounted wall-to-wall and the boundary layer was tripped on both sides at $x/c = 0.07$ from the leading edge for fully-turbulent behavior. The results showed that a periodic self-sustained shock-wave motion was only obtained at an angle of attack of 3.5° or higher, despite the fact that the first shock-wave unsteadiness occurred at 3.1°. Most of the results reported in that paper are for $\alpha = 3.5^\circ$, which makes the test case even more challenging since this incidence is close to the buffet onset boundary. The flow was shown to be essentially two dimensional, exhibiting a main frequency of 69 Hz (or a reduced frequency $2\pi fc/U \approx 0.41$), and the shock-wave motion was coupled with an intermittent separation of the boundary layer. According to the authors, the flow dynamics can be summarized as follows: when the shock is at its most upstream position, the boundary layer is separated from the foot of the shock to the trailing edge. As the shock starts moving downstream, the flow reattaches and remains attached during the shock excursion downstream, except maybe at the trailing edge. When the shock reaches its most downstream position, the boundary layer undergoes a progressive thickening until it separates again and the shock starts moving back upstream.

II. Turbulence modeling approach

The choice of the DDES is directly related to the main reasons that motivated the development of the method. In the case of a standard DES based on the Spalart-Allmaras model[22] or on one of its numerous modified versions, the turbulence length scale given by the RANS branch of the model is usually the distance to the closest wall, while that provided by the LES branch has only the largest local grid spacing as variable[21]. Hence, the switching between RANS and LES modes is driven by grid parameters only, it is thus invariant in time and independent from the flow physics. In the simulation of transonic buffet, the tangential grid spacing should be small enough for a proper resolution of the shock-wave motion region. This can reduce the RANS region to a thin layer around the airfoil when using DES on fine grids. Furthermore, the boundary layer is not permanently separated and becomes considerably thick due to the interaction with the shock wave and to the adverse pressure gradient on the rear part

of the airfoil. Therefore, the boundary layer thickness may get much larger than the RANS region provided by DES, which can result in an erroneous activation of the LES mode inside the boundary layer and potentially lead to modeled-stress depletion[20] (MSD). On the contrary, the redefinition of the turbulence length scale in DDES makes the method capable of detecting and protecting an attached boundary layer from the LES mode.

A. RANS model

The performance of a hybrid RANS-LES approach is directly related to the ability of its RANS branch in predicting separation and other key features of the flow near the wall. Preliminary two-dimensional computations of steady and unsteady transonic flows over the OAT15A airfoil near the buffet boundary have been conducted to assess several one- and two-equation eddy-viscosity models commonly used in aerodynamics. Regarding the first group, the Spalart-Allmaras model (SA), the Edwards-Chandra modified SA model[23] (EDW) and the Strain-Adaptive Linear Spalart-Allmaras model[24] (SALSA) were considered. For these models, additional computations were run adding the compressibility correction of Secundov[25] (+CC) to the transport equation. The correction acts as a destruction term, tending to lower the eddy-viscosity levels in turbulent regions of high deformation and velocity magnitude such as compressible mixing layers. Regarding two-equation closures, Menter's Baseline (BSL) and Shear Stress Transport (SST) models[26], the reformulated k-ω model of Wilcox[27] (KWW) as well as the k-ε model of Chien[28] (KEC) were considered. The results for the steady attached flows at $\alpha = 2.5^\circ$ and 3.0° (below the buffet onset boundary) showed that the shock-wave location is highly model-dependent and that most models tend to predict it too far downstream compared to the experimental data, as illustrated in figure 1 for $\alpha = 2.5^\circ$. At both incidences, the best predictions of the pressure coefficient distributions were obtained with the SST and SA models. The compressibility correction applied to the one-equation models moved the shock slightly upstream (closer the the experimental data) in all cases. Despite the reasonably good results obtained for steady flow using the SST and SA models, both failed in predicting the flow unsteadiness at $\alpha = 3.5^\circ$, leading to steady solutions. The KWW, EDW and SALSA models were successful in predicting self-sustained periodic flow, however, the shock-wave motion amplitude was too small with the KWW and EDW models and considerably overestimated with the SALSA model. Since the addition of the compressibility correction to a model tends to reduce its dissipative character, the resulting model can exhibit a very different behavior near the buffet boundary in comparison with the original. When applied to the SA model, the compressibility correction led to numerically unstable behavior. However, in conjunction with the more robust EDW model it resulted in rapid and smooth convergence. This closure gave the best agreement with the experimental data among the models evaluated, with the shock-wave motion range particularly well predicted despite a mean shock located somewhat downstream the experimental position (the results will be shown later in the text). Therefore, the Edwards model with compressibility correction (EDW+CC) has been selected for the DDES of the transonic buffet over the OAT15A airfoil in the present study.

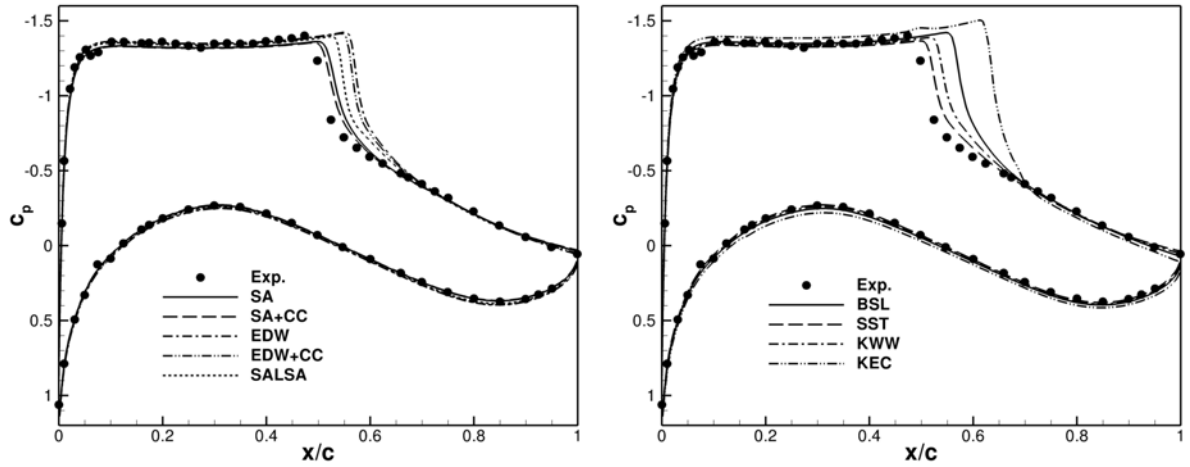

(a) One-equation models

(b) Two-equation models

Figure 1. Mean surface pressure distributions for the steady flow at $\alpha = 2.5^\circ$.

B. Hybrid model formulation

The adopted turbulence modeling approach has a single transport equation from the Edwards-Chandra model for the modified eddy viscosity $\tilde{\nu}$. By adding the compressibility correction of Secundov (last term on the right-hand side of Eq. (1)), one obtains:

$$\frac{D\tilde{\nu}}{Dt} = c_{b1}\tilde{S}\tilde{\nu} + \frac{1}{\sigma}\frac{\partial}{\partial x_k}\left[(\nu+\tilde{\nu})\frac{\partial\tilde{\nu}}{\partial x_k}\right] + \frac{c_{b2}}{\sigma}\frac{\partial\tilde{\nu}}{\partial x_k}\frac{\partial\tilde{\nu}}{\partial x_k} - c_{w1}f_w\left(\frac{\tilde{\nu}}{l}\right)^2 - c_5\frac{\tilde{\nu}^2}{a^2}\frac{\partial u_i}{\partial x_j}\frac{\partial u_i}{\partial x_j}, \tag{1}$$

where

$$\nu_t = \tilde{\nu} f_{v1}, \qquad f_{v1} = \frac{\chi^3}{\chi^3 + c_{v1}^3}, \qquad \chi = \frac{\tilde{\nu}}{\nu}, \tag{2}$$

$$\tilde{S} = S\left(\frac{1}{\chi} + f_{v1}\right), \qquad S = \left[\left(\frac{\partial u_i}{\partial x_j} + \frac{\partial u_j}{\partial x_i}\right)\frac{\partial u_i}{\partial x_j} - \frac{2}{3}\left(\frac{\partial u_k}{\partial x_k}\right)^2\right]^{\frac{1}{2}}, \tag{3}$$

$$f_w = g\left(\frac{1 + c_{w3}^6}{g^6 + c_{w3}^6}\right)^{1/6}, \qquad g = r + c_{w2}\left(r^6 - r\right), \qquad r = \frac{\tanh\left[\tilde{\nu}/\left(\tilde{S}\kappa^2 l^2\right)\right]}{\tanh 1.0}. \tag{4}$$

In the destruction term of Eq. (1), the DDES turbulence length scale l replaces the wall distance. This variable also appears in the function f_w through the near-wall parameter r, and is defined as:

$$l = d - f_d \max\left(0, d - C_{\text{DES}}\Delta_{\max}\right). \tag{5}$$

$\Delta_{\max} = \max\left(\Delta_x, \Delta_y, \Delta_z\right)$ is the largest local grid spacing and the constant C_{DES} is taken as 0.65 based on the study by Shur et al.[29] with the SA model in decaying homogenous isotropic turbulence. The delaying function f_d tends to 1 in LES regions (where $r_d \ll 1$) and to 0 everywhere else, and reads:

$$f_d = 1 - \tanh\left[\left(8r_d\right)^3\right], \qquad r_d = \frac{\nu_t + \nu}{S_d \kappa^2 d^2}, \qquad S_d = \sqrt{\frac{\partial u_i}{\partial x_j}\frac{\partial u_i}{\partial x_j}}. \tag{6}$$

As it can be seen in Eq. (6), the turbulence length scale in DDES is also function of the local state of the flow by means of the eddy viscosity and the deformation tensor. The remaining constants in the model are given by:

$$c_{v1} = 7.1, \qquad c_{b1} = 0.1355, \qquad c_{b2} = 0.622, \qquad \sigma = 2/3, \qquad \kappa = 0.41,$$

$$c_{w1} = \frac{c_{b1}}{\kappa^2} + \frac{1 + c_{b2}}{\sigma}, \qquad c_{w2} = 0.3, \qquad c_{w3} = 2, \qquad c_5 = 3.5.$$

III. Numerical aspects

A. Computational grid

The three-dimensional grid used in the present study consists of equally-spaced copies of a baseline planar grid in the spanwise direction, yielding constant Δ_z. The planar grid has a C-H topology and is similar to that employed by Deck[19] for the ZDES, which had approximately 110.000 cells. The farfield is located at a distance of 80 chords from the airfoil and the number of cells has been increased to about 130.000 in order to enhance the resolution of turbulent eddies. For the steady flow at 2.5° with the EDW+CC model, the y^+ coordinate is everywhere smaller than 0.5 on the present grid. The definition of the domain extent in the spanwise direction has followed the analogy made by Deck[19] between an airfoil of thickness e and a backward-facing step of height H. According to that author, in order to capture the largest spanwise wavelengths in the case of the flow past the step, a minimum width of $4H$ would be required. Assuming that for an airfoil at low incidence the maximum height of the separated region is about a half of the profile thickness ($e/2$), then a span L_z of approximately $2e$ would be a minimum. In the case of the OAT15A airfoil, this gives $L_z \approx 0.25\,c$ since $e = 0.123\,c$. Therefore, the domain extent in the spanwise direction has been set as $0.26\,c$ in the three-dimensional grid.

The other parameter to be chosen is the number of grid cells in the spanwise direction. In DDES, there is no reason for adopting a transverse grid spacing Δ_z much smaller than Δ_x since the length scale provided by the LES branch is based on the largest local grid spacing. Therefore, 64 cells have been distributed in z to obtain $\Delta_z \approx \Delta_x$ on the upper surface of the airfoil and in the near wake, giving a grid of about 8.3-million cells.

B. Numerical method

The CFD code used in the present work is the NSMB[30] (Navier Stokes Multi Block) code, which is a density-based multi-block structured finite volume solver for the Navier-Stokes equations. The convective fluxes have been discretized by means of a third-order Roe upwind scheme applying the MUSCL extrapolation and van Leer flux limiters. Time integration has been performed implicitly using the dual time stepping technique with 3 Gauss-Seidel iterations. A physical time step of 0.1 μs has been adopted ($\approx 1\times10^{-4}c/U$), which corresponds to a CFL number varying between 1 and 2.5 during buffet and is five times smaller than that used by Deck[19]. At each time step, convergence is evaluated upon the norm of the density residual with a tolerance of 1×10^{-3}, which ensures good convergence with the present time step. The freestream/ambient eddy viscosity has been set to $\tilde{\nu}/\nu = 4$, which is within the range recommended by Spalart and Rumsey[31] for one-equation models. To get closer to the experimental configuration, transition is enforced at $x/c = 0.07$ by imposing $\nu_t = 0$ upstream, though preliminary tests in two dimensions with different URANS models showed that accounting for the effects of that portion of

laminar boundary layer is not crucial. Because the computational domain considered is intended to represent only a small central part of the wind tunnel model, periodic conditions have been prescribed at the lateral boundaries.

In addition to the DDES, a two-dimensional URANS simulation with the EDW+CC model employing the same time step and numerical parameters has been conducted for comparison purpose. The methodology adopted in the simulations has been as follows: after several hundreds of iterations in steady mode (local time stepping) starting from a uniform flowfield initialized with freestream properties, a first unsteady (time-resolved) computation is performed. This latter lasts until the buffet phenomenon becomes fully developed, requiring about 7×10^5 time steps. Then, time is reset to zero and the computation of the permanent unsteady regime begins for sampling of the flow statistics. In the case of the DDES, 9 buffet periods (more than 1.1×10^6 time steps) have been computed and have proven to be sufficient to guarantee the convergence of the flow statistical properties. For the URANS simulation, 21 buffet cycles have been computed, which is equivalent to about 300 flow convective time units c/U.

IV. Results

A. Flow topology

As expected, the present DDES formulation led to self-sustained large-scale motion of the shock wave at the experimental angle of attack. The flow evolution during one period of buffet is depicted in figure 2, which presents the distribution of positive (black) and negative (white) values of the vorticity in the z-direction, on the mid-plane, at several time instants. $t^* = tU/c$ a non-dimensional time where $t^* = 0$ was set to an instant of maximum lift, with the shock wave at its most downstream position as illustrated in figure 2(a). At that moment, in addition to the separation bubble at the foot of the shock, rear separation also exists. These two grow simultaneously and eventually fuse into a large separation extending from the foot of the shock to the trailing edge. This scenario comes together with the initial stages of the shock-wave motion upstream, represented in figure 2(b). The figure also shows the presence of the von Kármán instability, which quickly gives rise to alternate vortex shedding where the coherent structures are initially purely two dimensional. Although there is no direct mention of such phenomenon in Ref.[6], von Kármán vortices were reported in several experiments on subsonic compressible flows around airfoils[32,33] as well as in the direct simulation of transonic buffet at lower Reynolds numbers by Bourdet et al.[34].

As the shock moves towards the leading edge, the height of the separated region increases progressively, causing a dramatic fall in the lift. During the motion, the wake develops a spanwise undulation. For better visualization of this process and particularly of the turbulent eddies resolved by the DDES, isosurfaces of vorticity magnitude at three instants are presented in figure 3. An early stage of the transition is shown in figure 3(a), whereas in figure 3(c) the flow is already strongly three-dimensional. The vortex structures organize according to a preferential spanwise wavelength as a consequence of the development of the secondary instability of the primary vortices. This was analyzed experimentally by Williamson[35] and in the direct simulations by Persillon et al.[36] and Bourdet et al.[34] for incompressible and transonic regimes, respectively. Besides the breakdown of the coherent structures, small eddies can be observed in the separated region in figure 3(c). The evolution of the surface pressure in the area downstream the shock is illustrated in figure 4. The wall pressure distribution changes from a strictly two-dimensional pattern to a three-dimensional one. As can be seen in the figure, the domain spanwise extent and the periodic conditions allow the resolution of eight wavelengths of the transverse undulation. Therefore, its actual wavelength can be estimated to be in the range $0.029-0.037c$.

Within each buffet period, the size of the cores of the coherent structures as well as the distance between two consecutive vortices vary considerably. These phenomena can be noticed by comparing the vortex streets in figures 2(b) and 2(g), for example, and follow the changes in the height of the separation region. In other words, the system composed by the airfoil and the viscous region around it defines a dynamic effective body whose signature evolves in time. Figure 2(d) corresponds to the instant when the shock wave is at its most upstream position and the boundary layer downstream it is fully separated. The instant of minimum lift, however, occurs a bit later after the shock has already started moving back downstream; it is illustrated in figure 2(f). The height of the separated region then decreases continuously and the boundary layer reattaches, suppressing the vortex shedding as seen in figures 2(g) and 2(h). As the shock reaches its most downstream position, the wake becomes steady again and the cycle restarts.

The time history of the lift coefficient after the transient period is presented in figure 5(a) for both the DDES and URANS simulations. Compared to URANS, the DDES is less regular and exhibits high-frequency secondary fluctuations produced mainly by the alternate vortex shedding when the flow separates. The mean lift coefficient for the DDES is lower than that of URANS (it drops from 0.956 to 0.934) and a slight reduction in the average amplitude of the main fluctuation is also noted. The Power Spectral Densities (PSD) of these two signals are given in figure 5(b) and indicate a main buffet frequency of 80.5 Hz for the DDES and 73.2 Hz for URANS (the experiments measured $f \approx 69$ Hz). Because the DDES signal is less regular and shorter than that of URANS, the peak in the DDES spectrum is not as well defined as in the URANS case. The secondary fluctuations create a 'bump' centered at approximately $35f$, suggesting that their frequency varies during buffet. This agrees with the observations made for figure 2 regarding the dynamics of the vortex street as the geometry of the effective body changes.

The trailing edge vortices that appear during separation are associated with the generation of upstream-moving

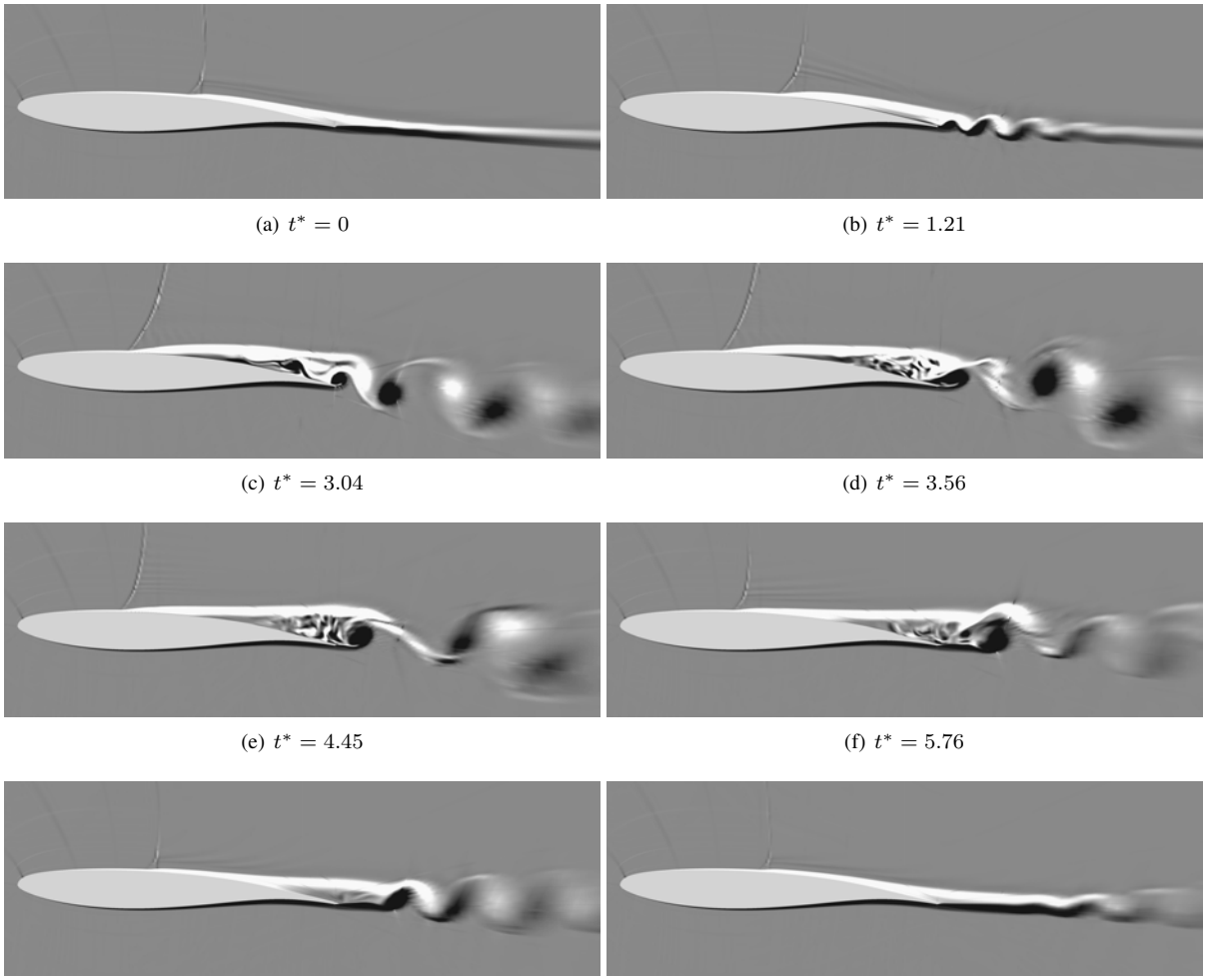

(a) $t^* = 0$ (b) $t^* = 1.21$

(c) $t^* = 3.04$ (d) $t^* = 3.56$

(e) $t^* = 4.45$ (f) $t^* = 5.76$

(g) $t^* = 7.70$ (h) $t^* = 9.07$

Figure 2. Instantaneous isocontours of spanwise vorticity on the mid-plane.

waves in the flow. As shown in the experimental work of Alshabu and Olivier[32], such waves are coupled with perturbations in the boundary layer that propagate downstream and interact with the trailing edge and the wake. The time history of the wall pressure at $x/c = 0.45$ on the upper surface presented in figure 6 reveals that the higher-frequency oscillations observed in the experimental signal are well captured by the present DDES, while the URANS signal remains regular and smooth. These secondary pressure oscillations appear when the shock is located upstream the given position and correspond to the same frequency range of the the bump in figure 5(b).

In order to better understand the flow topology, the intermittent separation/reattachment process that takes place over the airfoil is investigated in more detail. Figure 7 presents a map of flow separation during buffet as predicted by the DDES and URANS approaches. The abscissa corresponds to the position from the leading edge along the upper surface and the ordinate to the non-dimensional time normalized by the duration of the buffet period (which is different for each model). Contrary to the convention adopted in the previous figures, in figure 7, $t = 0$ corresponds to instants of minimum lift. The flow condition (attached or separated) at a given position and time instant has been determined by evaluating the spanwise vorticity at the wall. The dark zones in the figures represent reverse flow, whereas the white ones indicate that the flow is attached to the surface. Because the URANS simulation resulted in a periodic flow, the distribution shown in figure 7(a) repeats indefinitely with insignificant changes. The results illustrated in figure 7(b) for the DDES refer to a unique period instead. Nevertheless, the distribution shown in the figure is representative of all other periods, which may exhibit only some quantitative variations. At minimum lift ($t = 0$), the shock wave is in the early stages of its motion downstream. While the flow predicted by the URANS simulation at that instant is completely separated downstream the shock, the DDES gives an almost fully attached flow over the same region. For both models the boundary layer remains attached during the shock-wave motion downstream except by the separation bubble at the foot of the shock, which seems to be smaller in URANS. The figures also reveal that while the shock excursion upstream takes approximately a half of the buffet period in URANS, it represents only one-third of the cycle in the case of the DDES, which may explain the higher buffet frequency found for that method. As the shock approaches its most downstream position, an important difference regarding the development of separation is noted. According to the URANS simulation, flow separation clearly evolves from the foot of the shock towards the trailing edge. On the contrary, figure 7(b) confirms that, in the case of the DDES, the separation bubble and the rear separation grow simultaneously, joining each other around $x/c = 0.75$ to create a single large separation.

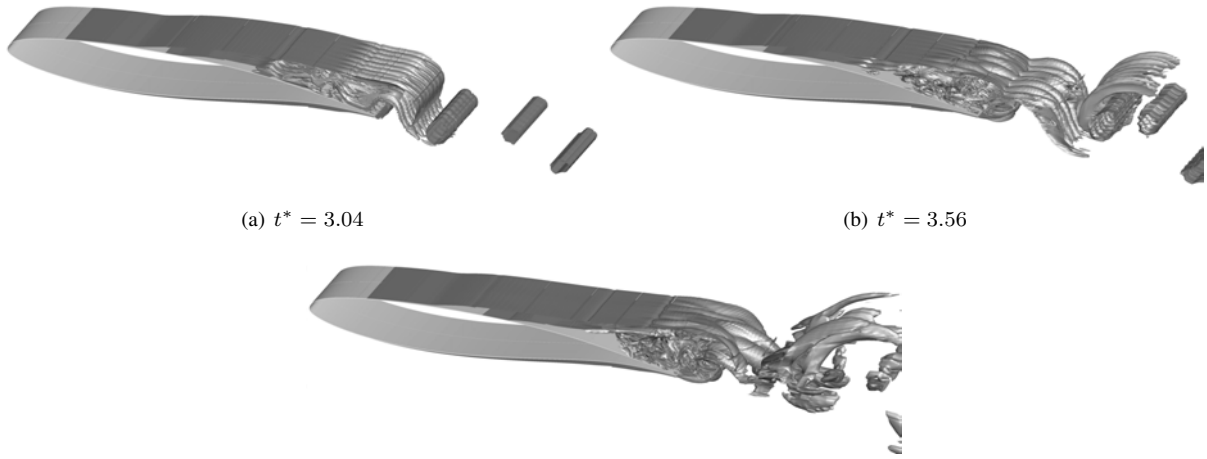

(a) $t^* = 3.04$ (b) $t^* = 3.56$

(c) $t^* = 4.45$

Figure 3. Instantaneous vorticity magnitude isosurfaces for $|\Omega|\, c/U = 10$.

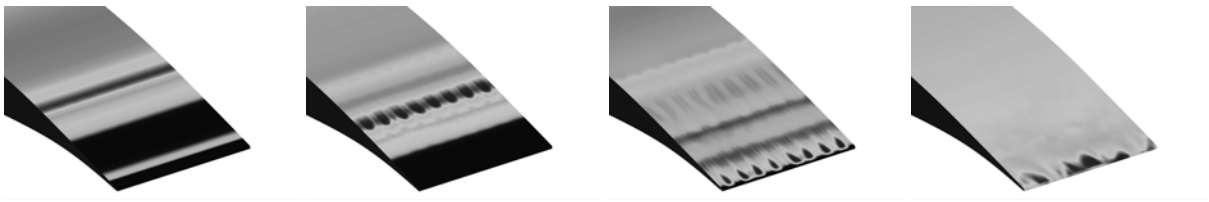

(a) $t^* = 2.57$ (b) $t^* = 2.88$ (c) $t^* = 3.09$ (d) $t^* = 3.51$

Figure 4. Surface pressure distributions behind the shock (qualitative).

As the shock wave moves back upstream, the size of the separated area increases accordingly. During this part of the buffet cycle, the DDES pattern near the trailing edge that is not random. The small white areas close to $x/c = 1$ are indeed the signature of the alternate vortices, and their continuously increasing size and spacing also emphasize the transformation of the effective body seen by the flow.

B. Statistical flow properties

1. Surface pressure

Figure 8(a) compares the mean pressure coefficient distributions obtained with the DDES and URANS approaches with the experimental data. On the upper surface, the spread compression after the supersonic plateau gives an idea of the the shock-wave excursion. In that region, the slopes of the DDES and URANS curves suggest similar shock-wave motion ranges. However, the mean shock position of the DDES is located more upstream and closer to the experimental data than that of the URANS computation. Nevertheless, the pressure recovery region on the rear part of the airfoil in the DDES gets flattened, yielding a trailing edge pressure that is lower than in the experiments. Both numerical solutions give good agreement over the lower surface, where the flow during buffet remains always attached and subcritical. The distributions of the RMS of the pressure fluctuations on the upper surface is illustrated in figure 8(b). The zone where the highest RMS levels take place results from the shock-wave oscillation and is another indicator of its motion range, with the peak being a rough estimate of the mean shock-wave position. Upstream that zone, the fluctuations are very low and agree well with the levels measured in the experiments whatever the model. As already evidenced by means of figure 8(a), the shock-wave motion range predicted by the DDES is closer to the experimental one, and the maximum fluctuation is slightly lower than that of URANS. Just downstream the shock-motion region, the experimental data exhibits an almost flat distribution. This behavior is not predicted by any of the simulations. Moreover, as one approaches the trailing edge, the pressure fluctuations obtained with the DDES get more and more overestimated, whereas the URANS simulation agrees better with the experiments. The increase in the fluctuations is mainly caused by the impingement of large-scale structures near the trailing edge.

2. Velocity field

Figure 9 presents the mean profiles of the longitudinal velocity component at four stations on the upper surface of the airfoil. At $x/c = 0.28$, the flow is always ahead of the shock wave and remains always attached during buffet, and both the DDES and URANS computations predict well the experimental profile. The station at $x/c = 0.45$ lies inside the shock-wave motion range and is close to the mean shock position for the DDES and the experiments.

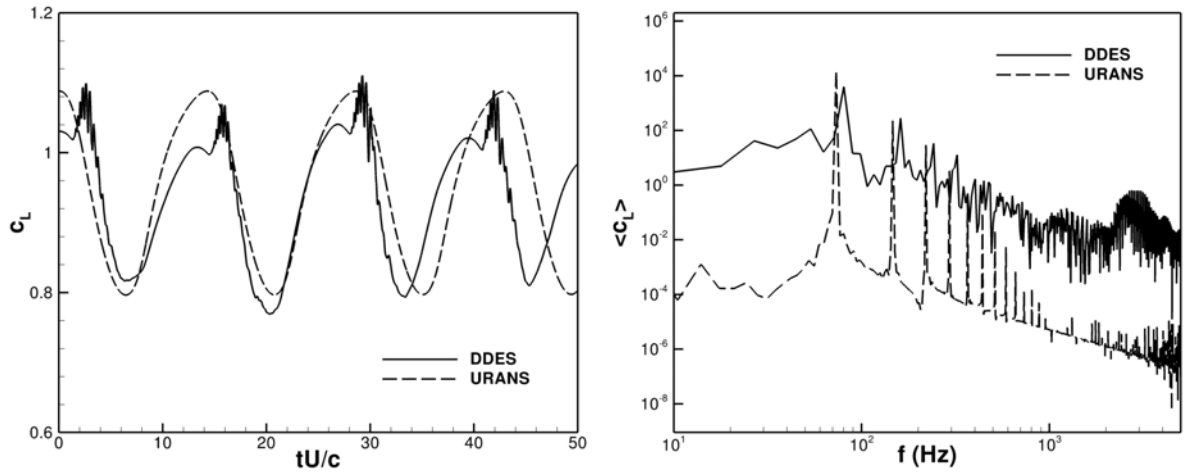

(a) Temporal evolution (b) PSD

Figure 5. Time history and Power Spectral Density of the lift coefficient.

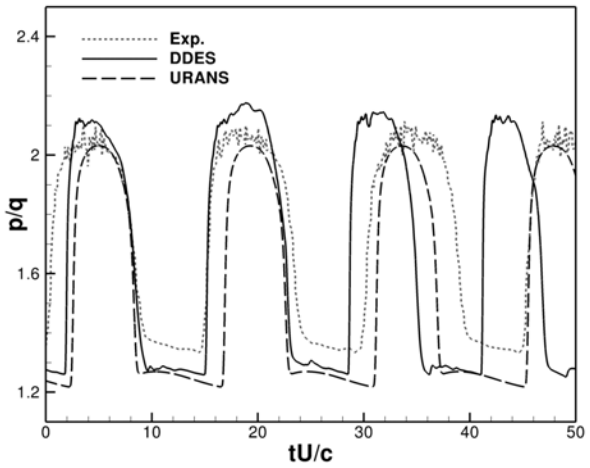

Figure 6. Time history of pressure at $x/c = 0.45$.

A deficit in the outer velocity can be observed for the DDES, which also shows a mean boundary layer that is thicker than the experimental one. The URANS profile is in better agreement with the experiments despite the fact that the method predicts the shock/wave boundary layer interaction somewhat downstream. The location at $x/c = 0.60$ is always behind the shock wave. There, none of the simulations correctly predict the experimental curve below $y/c = 0.02$. Moreover, the DDES fails in predicting a mean reverse flow as seen in the experimental data and the URANS profile is only barely separated. As the distance from the wall increases, the URANS results get closer to the experimental distribution. Further downstream at $x/c = 0.75$, both numerical simulations show good prediction.

The profiles for the RMS of the longitudinal velocity fluctuations at the same four stations are given in figure 10. Both the DDES and URANS lead to almost zero unsteadiness at $x/c = 0.28$. Inside the shock-wave motion region at $x/c = 0.45$, the models overestimate the fluctuation levels over the whole profile. The URANS simulation is closer to the experimental data than the DDES. Downstream that zone, the performance of the turbulence models improves as one moves downstream. At $x/c = 0.60$, the RMS levels are reasonably well predicted. While the URANS approach gives good results below $y/c = 0.04$, it does not reproduce the experimental outer velocity. As for the mean profiles, at $x/c = 0.75$ the agreement between URANS and experiments is remarkable.

Figure 11 illustrates the distributions of the RMS of the longitudinal velocity fluctuations around the airfoil as predicted by the two methods. It reveals that the highest fluctuations take place in the shock wave/boundary layer interaction and in the near wake. Furthermore, the trend noted in figures 8(b) and 10 concerning the overall enhancement of the fluctuations of the flow properties by the DDES is clearly visible. However, compared to URANS, a slight decrease in the RMS levels in the area of shock-wave motion external to the boundary layer can be observed. The largest differences between the two models are noticed in the near wake, where strong velocity oscillations exist in the case of the DDES. These become clearer when looking at the distributions of the vertical component of the fluctuations, which are shown in figure 12. The differences around the trailing edge are mainly a result of the alternate vortex shedding, which does not exist in the URANS simulation.

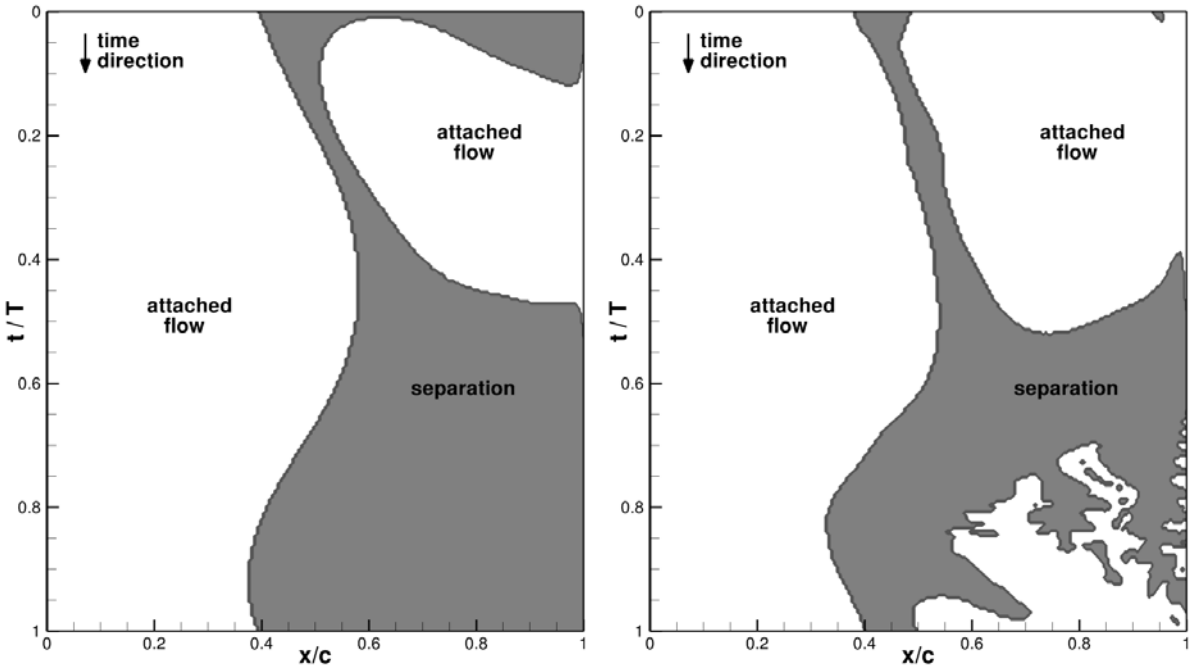

(a) URANS (b) DDES

Figure 7. Spatio-temporal evolution of flow separation on the upper surface.

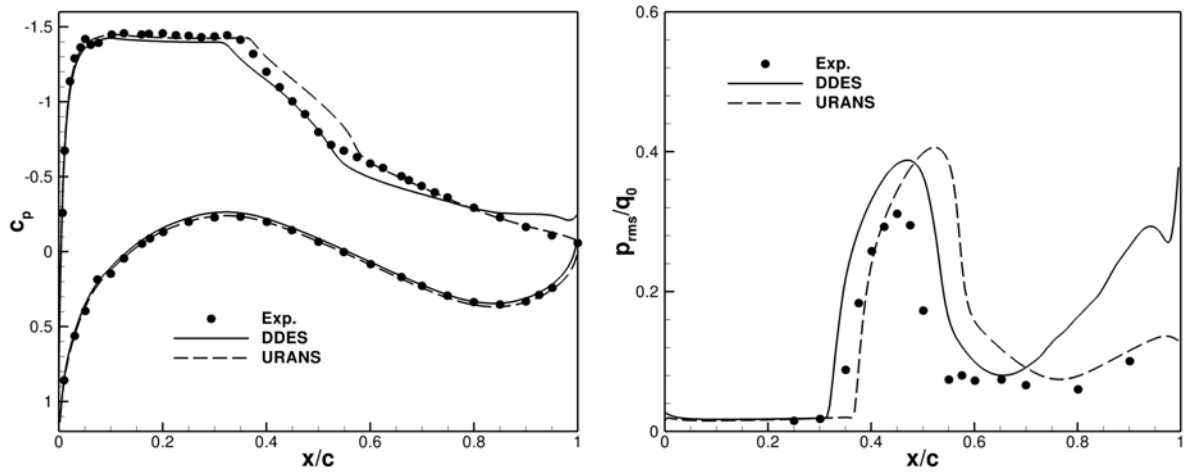

(a) Mean pressure coefficient (b) RMS of the fluctuations on the upper surface

Figure 8. Surface statistical pressure distributions around the airfoil.

C. Analysis of the DDES behavior

1. RANS and LES regions

An important issue is how the DDES switches between RANS and LES modes when submitted to different flow topologies during buffet (i.e., attached flow and shock-induced separated flow). RANS and LES zones can be distinguished by means of the function f_d, which determines the length scale of the model in Eq. (5). The function was designed to be close to 1 in LES regions and to 0 in RANS as well as to provide a rapid change between the two modes. The distributions of the function $(1 - f_d)$ around the OAT15A airfoil is illustrated in figure 13 at maximum lift with the shock at its most downstream position and with the shock at its most upstream position. By the color scale adopted, the black zones correspond to RANS areas whereas the white zones are computed through LES. Any shade of gray in-between is situated within the zone of transition. Overall, the RANS layer around the airfoil generated by the DDES is much thicker than that of a standard DES on the present grid as it will be shown later. This is particularly true in the region between the shock wave and the trailing edge, where the attached boundary layer undergoes the effects of the interaction with the shock and the adverse pressure gradient. When the shock is at its most downstream position (figure 13(a)) most of the boundary layer is attached. At that instant, the distribution of f_d is smooth and follows the thickening of the boundary layer over the upper and lower surfaces because of the definition of the near-wall parameter r_d.

Figure 14 shows the instantaneous wall profiles of the function f_d, the eddy-viscosity ratio μ_t/μ and velocity

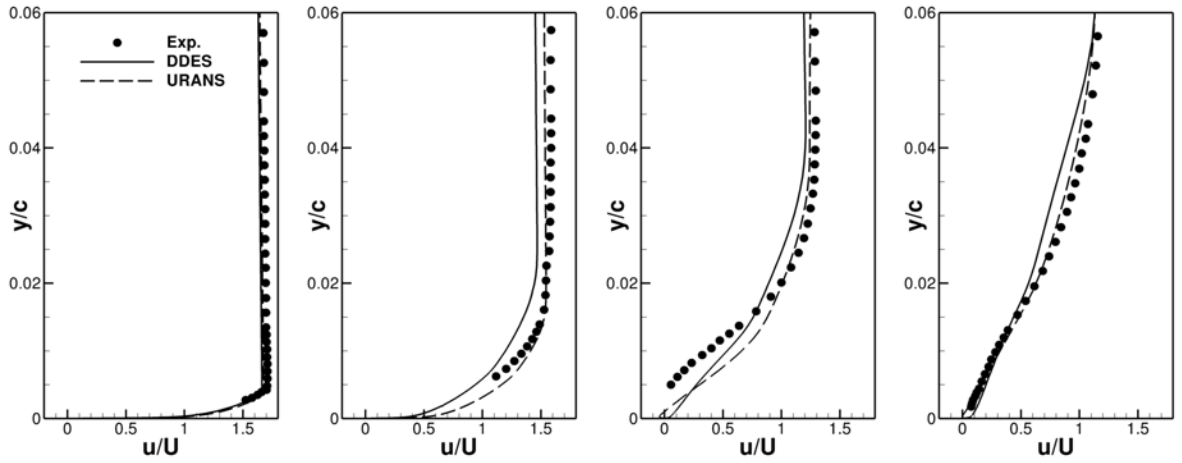

(a) $x/c = 0.28$ (b) $x/c = 0.45$ (c) $x/c = 0.60$ (d) $x/c = 0.75$

Figure 9. Mean longitudinal velocity profiles on the upper surface.

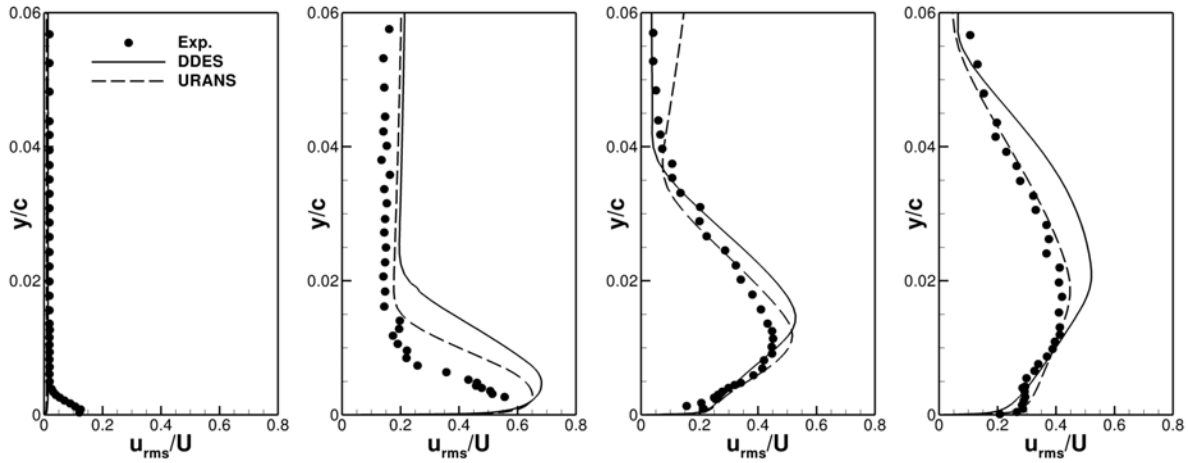

(a) $x/c = 0.28$ (b) $x/c = 0.45$ (c) $x/c = 0.60$ (d) $x/c = 0.75$

Figure 10. RMS profiles of the longitudinal velocity fluctuations.

at four locations on the upper surface. Also, for comparison, the position where a standard DES would switch from RANS to LES (where $l_{\text{RANS}} = l_{\text{LES}}$) on the present grid is represented by a horizontal dash-dot-dot line. One thing that can be immediately noticed is that all stations present irregularities in the f_d profiles. These arise just outside the boundary layer where the magnitude of the deformation tensor becomes very small, increasing r_d abruptly. Then, as the wall distance increases further, r_d goes to zero and f_d smoothly tends to 1 as desired. The irregularities in the f_d distribution are visible in figure 13, under the form of thin dark layers outside the main RANS layer on both sides of the airfoil. Nonetheless, because they arise only outside the viscous layer they have no appreciable effect on the eddy viscosity distribution (and, for this reason, they are not problematic). The profiles evidence that the DDES method ensures that near-wall regions where high velocity gradients take place are treated in RANS. As a matter of fact, upstream the shock at $x/c = 0.28$, the DES approach would also provide a proper switching to LES. However, at $x/c = 0.45$, it would activate the LES mode inside the boundary layer, whereas the DDES yields a satisfactory gradual transition. The differences between the two approaches get larger at $x/c = 0.60$, which lies well inside the separation bubble. At $x/c = 0.75$, the boundary layer is particularly thick and the tangential grid spacing relatively small. As can be seen in the figure, a DES would switch to LES at low values of y_w. On the contrary, the DDES method guarantees that the major part of the boundary layer is treated in RANS.

The distribution of RANS and LES regions when the shock wave is at its most upstream position (largest extent of separation) is illustrated in figure 13(b). At that instant, the shock is approximately located at $x/c = 0.32$ and the flow downstream is separated. Disturbances in the f_d distribution appear just above the shear layer and give an idea about the height of the separation. As desired, the bulk of that region is treated in LES. Figure 15 reveals that the wall profiles at $x/c = 0.28$ are very similar to those of when the shock is downstream, as the boundary at that position stays always attached. At $x/c = 0.45$, 0.60 and 0.75, the flow is separated and the thicknesses of the RANS layers are larger than in figure 14 for attached flow and than in the case of DES. Nevertheless, the f_d function yields rapid switching to LES in all three cases.

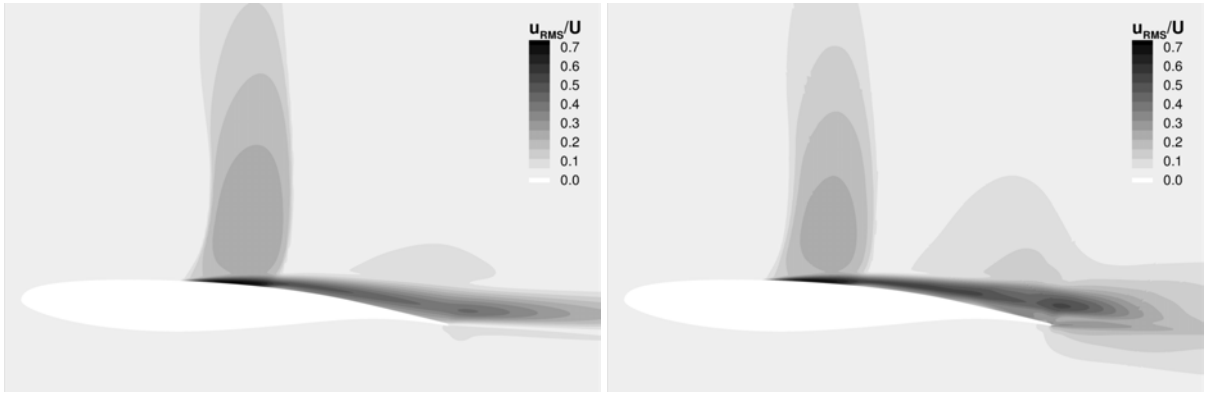

(a) URANS (b) DDES

Figure 11. Spatial distribution of the RMS values of the longitudinal velocity fluctuations.

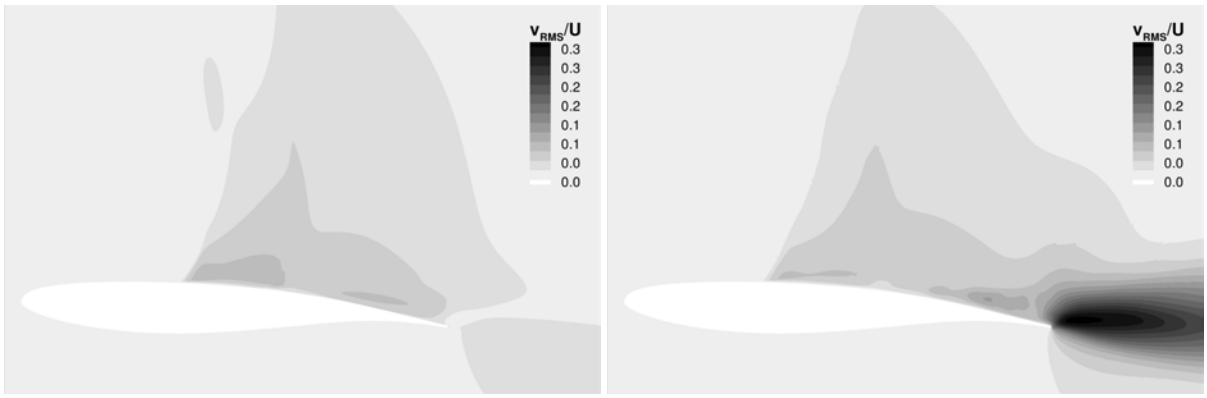

(a) URANS (b) DDES

Figure 12. Spatial distribution of the RMS values of the vertical velocity fluctuations.

2. Discussion

The DDES results differ considerably from those of the URANS simulation using the same RANS model. Differences are observed mostly in the shock wave/boundary layer interaction region, over the rear part of the airfoil where intermittent separation occurs and specially near the trailing edge, where high levels of fluctuations of the flow properties are noted. Nonetheless, the investigation of the distribution of RANS and LES regions during buffet showed that the DDES ensures that the boundary layer is always treated in RANS, even when it gets very thick. In the sequence presented in figure 2, however, it can be seen that there is some delay in the formation of resolved structures when the flow separates. This is illustrated in figure 16, which shows two instantaneous isosurfaces of the Q-criterion, $Q = \frac{1}{2}\left(|\Omega|^2 - |S|^2\right)$. Despite the separation at the foot of the shock wave, a long distance is needed for the development of turbulent eddies on the rear part of the airfoil and in the shear layer. This phenomenon is common of hybrid RANS-LES computations when applied to flows where separation occurs naturally on smooth surfaces (instead of being driven by some geometry feature such as a spoiler or the edge of a backward-facing step, for example) and with no initial turbulent content. In DDES, this effect is particularly intensified as the RANS-mode layer around the airfoil is relatively thick even when the flow is separated as revealed by the f_d distributions in figures 13(b) and 15. Also, the overall grid refinement may also be associated with the DDES results as it is not clear if the cutoff length scale stays always in the inertial subrange of the turbulence spectrum in LES regions.

A comparison between the results of the present DDES and those of the Zonal Detached-Eddy Simulation (ZDES) of Deck[19] on the same configuration is given in figure 17, and helps supporting the above considerations. In that ZDES, the MSD issue was avoided by imposing RANS treatment (with the original SA model) in regions where the grid spacing in the direction normal to the wall was smaller than in the spanwise direction, what included the whole shock wave/boundary layer interaction. Moreover, LES regions used the standard subgrid length scale of LES, $\Delta = (\Delta_x \Delta_y \Delta_z)^{\frac{1}{3}}$, and had all near-wall functions in the turbulence model suppressed. As can be seen in figure 17(a), the mean pressure profiles have the same basic features, exhibiting flattened pressure recovery regions and lower pressure levels at the trailing compared to the experiments. The present DDES has provided a better prediction of the shock-wave motion region and of the pressure recovery area, being everywhere closer to the experimental data than the ZDES. However, because of the multiple differences in the modeling approach, numerical method, time step and grid resolution (somewhat finer in the present DDES), the comparison cannot be

(a) Shock downstream ($t^* = 0$) (b) Shock upstream ($t^* = 3.56$)

Figure 13. Instantaneous distributions of the function $1 - f_d$.

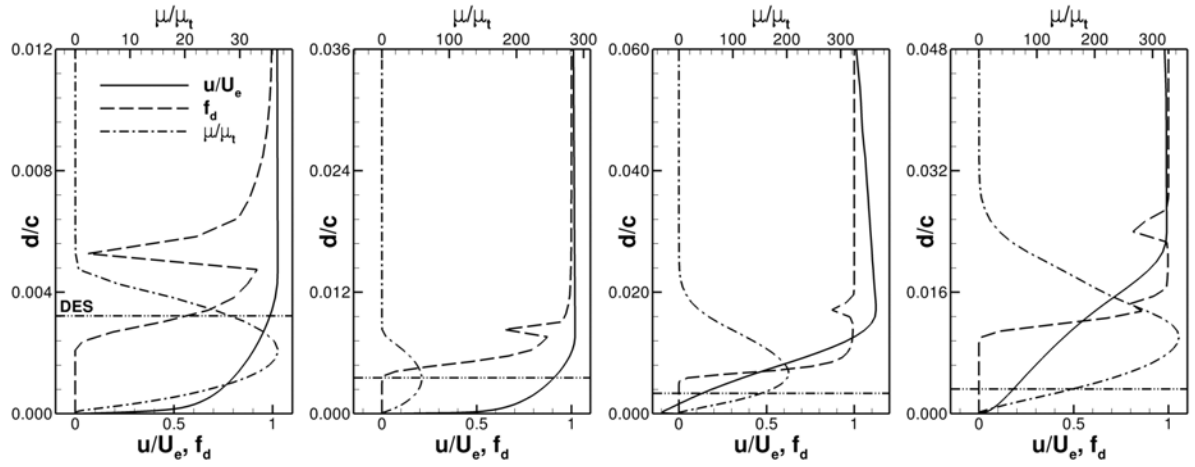

(a) $x/c = 0.28$ (b) $x/c = 0.45$ (c) $x/c = 0.60$ (d) $x/c = 0.75$

Figure 14. Profiles with the shock at its most downstream location ($t^* = 0$).

used to affirm the superiority of one method over the other for the present case. The pressure fluctuations shown in figure 17(b) reveal that the maximum levels predicted by the two approaches are similar despite some differences in the mean shock-wave position and motion range. As one approaches the trailing edge, the fluctuations predicted by the DDES get more intense than those of ZDES. This can be partially explained by the fact that the hybrid RANS-LES formulation in that ZDES was applied only over the upper surface and in the wake. This undoubtedly influences the trailing edge unsteadiness and probably prevents the alternate vortex shedding.

V. Conclusion

The transonic buffet flow over the OAT15A supercritical airfoil was simulated using a DDES approach based on a one-equation closure. The results were compared to experimental data as well as to a URANS simulation using the same RANS model. The models successfully predicted the self-sustained shock-wave/boundary layer interaction with an intermittent large-scale separation. While in URANS this separation evolves from the bubble at the foot of the shock wave to the tailing edge, rear separation is also exists and develops in the DDES. When the shock moves upstream and the flow separates, alternate vortex shedding takes place in the DDES flow exhibiting initially two-dimensional coherent structures that develop a secondary instability and quickly become three dimensional. The von Kármán vortices affect even the global forces and have a frequency several times higher than that of buffet; this frequency varies in time as the height of the wake changes. The DDES also captured secondary fluctuations of the flow properties in the boundary layer, which are related to wave propagation phenomena in the flowfield.

Statistical pressure distributions showed that the shock-wave location is well predicted by the DDES. Nevertheless, the pressure recovery area gets somewhat flattened with a low trailing-edge pressure. Moreover, as one moves towards the trailing edge, the fluctuations of the flow properties get overestimated by the DDES. Over the same region, the URANS computation is in better agreement with the experiments. The analysis of the distributions of the RANS and LES regions of DDES under different flow topologies during buffet showed that the method avoids MSD even when the boundary layer becomes considerably thick.

Acknowledgments

This work was supported by the ATAAC project - Advanced Turbulence Simulation for Aerodynamic Application Challenges (Seventh Framework Programme) - and by the ANR (Agence Nationale de Recherche) Cosinus "calcul intensif et simulation" ECINADS - Unsteady Turbulent and Adjoint Flows in High Performance Numerical Simulation. The authors gratefully acknowledge the french computing centers CALMIP and CINES for the resources allocated.

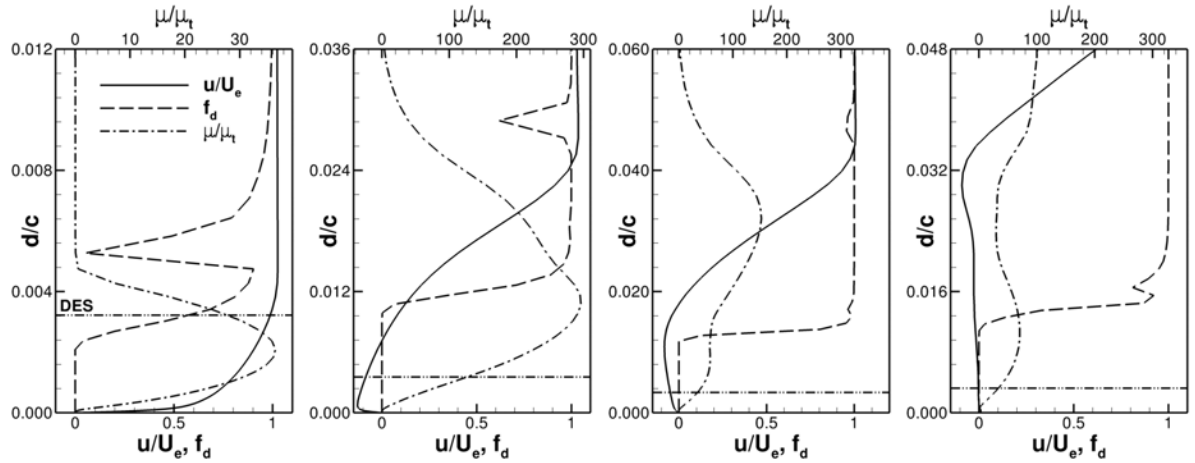

(a) $x/c = 0.28$ (b) $x/c = 0.45$ (c) $x/c = 0.60$ (d) $x/c = 0.75$

Figure 15. Profiles with the shock at its most upstream location ($t^* = 3.56$).

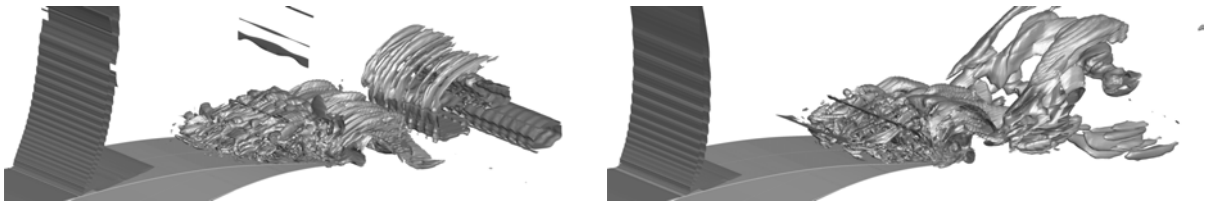

(a) $t^* = 3.56$ (b) $t^* = 4.45$

Figure 16. Instantaneous Q-criterion isosurfaces for $Q(c/U)^2 = 75$.

References

[1]McDevitt, J. B., Jr., L. L. L., and Deiwert, G. S., "Transonic Flow About a Thick Circular-Arc Airfoil," *AIAA Journal*, Vol. 14, No. 5, 1976, pp. 606–613.

[2]Seegmiller, H. L., Marvin, J. G., and Jr., L. L. L., "Steady and Unsteady Transonic Flow," *AIAA Journal*, Vol. 16, No. 12, 1978, pp. 1262–1270.

[3]Roos, F. W., "Some Features of the Unsteady Pressure Field in Transonic Airfoil Buffeting," *Journal of Aircraft*, Vol. 17, No. 11, 1980, pp. 781–788.

[4]Lee, B. H. K. and Ohman, L. H., "Unsteady Pressures and Forces During Transonic Buffeting of a Supercritical Airfoil," *Journal of Aircraft*, Vol. 21, No. 8, 1984, pp. 439–441.

[5]Lee, B. H. K. and Tang, F. C., "Transonic Buffet of a Supercritical Airfoil and Trailing-Edge Flap," *Journal of Aircraft*, Vol. 26, No. 5, 1989, pp. 459–464.

[6]Jacquin, L., Molton, P., Deck, S., Maury, B., and Soulevant, D., "Experimental Study of Shock Oscillation over a Transonic Supercritical Profile," *AIAA Journal*, Vol. 47, No. 9, 2009, pp. 1985–1994, also AIAA Paper 2005–4902, Jun. 2005.

[7]Lee, B. H. K., "Oscillatory Shock Motion Caused by Transonic Shock Boundary-Layer Interaction," *AIAA Journal*, Vol. 28, No. 5, 1990, pp. 942–944.

[8]Crouch, J. D., Garbaruk, A., Magidov, D., and Travin, A., "Origin of transonic buffet on aerofoils," *Journal of Fluid Mechanics*, Vol. 628, 2009, pp. 357–369.

[9]Levy Jr., L. L., "Experimental and Computational Steady and Unsteady Transonic Flows about a Thick Airfoil," *AIAA Journal*, Vol. 16, No. 6, 1978, pp. 564–572.

[10]Bouhadji, A. and Braza, M., "Organised modes and shockvortex interaction in unsteady viscous transonic flows around an aerofoil: Part I: Mach number effect," *Computers & Fluids*, Vol. 32, No. 9, 2003, pp. 1233–1260.

[11]Bouhadji, A. and Braza, M., "Organised modes and shockvortex interaction in unsteady viscous transonic flows around an aerofoil: Part II: Reynolds number effect," *Computers & Fluids*, Vol. 32, No. 9, 2003, pp. 1261–1281.

[12]Barakos, G. and Drikakis, D., "Numerical simulation of transonic buffet flows using various turbulence closures," *International Journal of Heat and Fluid Flow*, Vol. 21, 2000, pp. 620–626.

[13]Xiao, Q. and Tsai, H. M., "Numerical Study of Transonic Buffet on a Supercritical Airfoil," *AIAA Journal*, Vol. 44, No. 3, 2006, pp. 620–628.

[14]Thiery, M. and Coustols, E., "Numerical prediction of shock induced oscillations over a 2D airfoil: influence of turbulence modelling and test section walls," *International Journal of Heat and Fluid Flow*, Vol. 27, 2006, pp. 661–670.

[15]Iovnovich, M. and Raveh, D. E., "Reynolds-Averaged NavierStokes Study of the Shock-Buffet Instability Mechanism," *AIAA Journal*, Vol. 50, No. 4, 2012, pp. 880–890.

[16]Fröhlich, J. and von Terzi, D., "Hybrid LES/RANS methods for the simulation of turbulent flows," *Progress in Aerospace Sciences*, Vol. 44, 2008, pp. 349–377.

[17]Peng, S.-H., Doerffer, P., and Haase, W., editors, *Progress in Hybrid RANS-LES Modelling*, Vol. 111 of *Notes on Numerical Fluid Mechanics and Multidisciplinary Design*. Springer, 2010, Papers Contributed to the 3rd Symposium on Hybrid RANS-LES Methods, Gdansk, Poland, June 2009.

[18]Fu, S., Haase, W., Peng, S.-H., and Schwamborn, D., editors, *Progress in Hybrid RANS-LES Modelling*, Vol. 117 of *Notes on Numerical Fluid Mechanics and Multidisciplinary Design*. Springer, 2012, Papers Contributed to the 4th Symposium on Hybrid RANS-LES Methods, Beijing, China, September 2011.

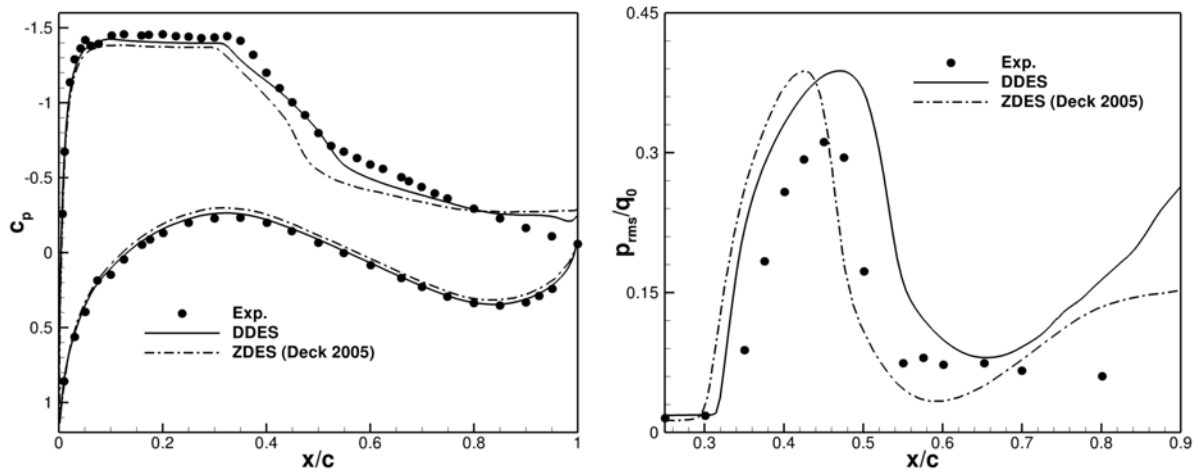

(a) Mean pressure coefficient

(b) RMS of the pressure fluctuations

Figure 17. Comparison between two different hybrid RANS-LES approaches.

[19]Deck, S., "Numerical Computation of Transonic Buffet over a Supercritical Airfoil," *AIAA Journal*, Vol. 43, No. 7, 2005, pp. 1556–1566.

[20]Spalart, P. R., Deck, S., Shur, M. L., Squires, K. D., Strelets, M. K., and Travin, A., "A new version of detached-eddy simulation, resistant to ambiguous grid densities," *Theoretical and Computational Fluid Dynamics*, Vol. 20, 2006, pp. 181–195.

[21]Spalart, P. R., Jou, W.-H., Strelets, M., and Allmaras, S., "Comments on the feasibility of LES for wings, and on a hybrid RANS/LES approach," *Advances in LES/DNS*, edited by C. Liu and Z. Liu, Greyden Press, Louisiana Tech University, 1997, pp. 137–147.

[22]Spalart, P. R. and Allmaras, S. R., "A one-equation turbulence model for aerodynamic flows," *La Recherche Aérospatiale*, Vol. 1, 1994, pp. 5–21.

[23]Edwards, J. R. and Chandra, S., "Comparison of Eddy Viscosity-Transport Turbulence Models for Three-Dimensional, Shock-Separated Flowfields," *AIAA Journal*, Vol. 34, No. 9, 1996, pp. 756–763.

[24]Rung, T., Bunge, U., Schatz, M., and Thiele, F., "Restatement of the Spalart-Allmaras Eddy-Viscosity Model in Strain-Adaptive Formulation," *AIAA Journal*, Vol. 41, No. 7, 2003, pp. 1396–1399.

[25]Spalart, P. R., "Trends in Turbulence Treatments," AIAA Paper 2000-2306, 2000.

[26]Menter, F. R., "Two-Equation Eddy-Viscosity Turbulence Models for Engineering Applications," *AIAA Journal*, Vol. 32, No. 8, 1994, pp. 1598–1605.

[27]Wilcox, D. C., "Formulation of the k-ω Turbulence Model Revisited," *AIAA Journal*, Vol. 46, No. 11, 2008, pp. 2823–2838.

[28]Chien, K.-Y., "Predictions of Channel and Boundary-Layer Flows with a Low-Reynolds-Number Turbulence Model," *AIAA Journal*, Vol. 20, No. 1, 1982, pp. 33–38.

[29]Shur, M., Spalart, P., Strelets, M., and Travin, A., "Detached-eddy simulation of an airfoil at high angle of attack," *Engineering Turbulence Modelling and Experiments*, Vol. 4, 1999, pp. 669–678.

[30]Vos, J. B., Rizzi, A. W., Corjon, A., Chaput, E., and Soinne, E., "Recent Advances in Aerodynamics Inside the NSMB (Navier Stokes Multi Block) Consortium," AIAA Paper 98-0225, 1998.

[31]Spalart, P. R. and Rumsey, C. L., "Effective Inflow Conditions for Turbulence Models in Aerodynamic Calculations," *AIAA Journal*, Vol. 45, No. 10, 2007, pp. 2544–255.

[32]Alshabu, A. and Olivier, H., "Unsteady Wave Propagation Phenomena on a Supercritical Airfoil," *AIAA Journal*, Vol. 46, No. 8, 2008, pp. 2066–2073.

[33]Fung, Y. C., *An Introduction to the Theory of Aeroelasticity*, Dover, 2002, Schlieren picture page 313 by D. W. Holder, National Physical Laboratory, England.

[34]Bourdet, S., Bouhadji, A., Braza, M., and Thiele, F., "Direct Numerical Simulation of the Three-Dimensional Transition to Turbulence in the Transonic Flow around a Wing," *Flow, Turbulence and Combustion*, Vol. 71, 2003, pp. 203–220.

[35]Williamson, C. H. K., "Three-dimensional wake transition," *Journal of Fluid Mechanics*, Vol. 328, 1996, pp. 345–407.

[36]Persillon, H. and Braza, M., "Physical analysis of the transition to turbulence in the wake of a circular cylinder by three-dimensional NavierStokes simulation," *Journal of Fluid Mechanics*, Vol. 365, 1998, pp. 23–88.